

Hydrophilic/Hydrophobic Interphase-Mediated Bubble-like Stretchable Janus Ultrathin Films toward Self-Adaptive and Pneumatic Multifunctional Electronics

Peng Xiao,^{†,‡} Yun Liang,^{†,‡} Jiang He,^{†,‡} Lei Zhang,^{*,†} Shuai Wang,^{†,‡} Jincui Gu,[†] Jiawei Zhang,^{†,‡} Youju Huang,^{†,‡} Shiao-Wei Kuo,[§] and Tao Chen^{*,†,‡}

[†]Key Laboratory of Marine Materials and Related Technologies, Zhejiang Key Laboratory of Marine Materials and Protective Technologies, Ningbo Institute of Material Technology and Engineering, Chinese Academy of Sciences, Zhongguan West Road 1219, 315201 Ningbo, China

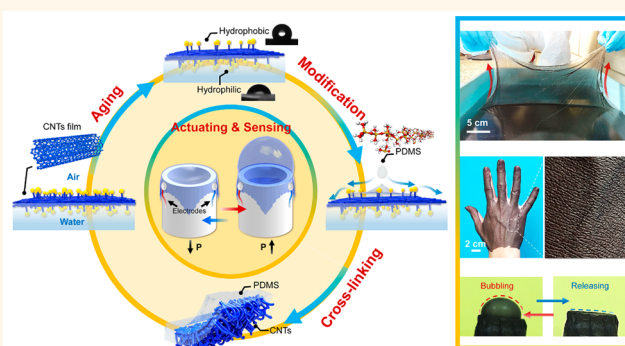
[‡]University of Chinese Academy of Science, Beijing 100049, China

[§]Department of Material and Optoelectronic Science, Center of Crystal Research, National Sun Yat-Sen University, 804 Kaohsiung, Taiwan

Supporting Information

ABSTRACT: As promising candidates for intelligent biomimetic applications similar to living organisms, smart soft materials have aroused extensive interest due to their extraordinarily designable structures and functionality. Herein, a bubble-like elastomer-based electronic skin that can be pneumatically actuated is achieved through hydrophilic/hydrophobic interphase mediated asymmetric functionalization. The asymmetric and controllable introduction of elastic polydimethylsiloxane into the carbon nanotube film at the air/water interface can endow the Janus ultrathin film with tunable conductivity, self-adhesivity, self-adaptivity, and even self-sealing properties. As a result, the Janus films can be employed as multifunctional electronics, including self-adhesive strain sensing/thermal managing devices and even noncontact mechanical sensors as artificial eardrums for tiny air-pressure detection. Significantly, these excellent features can further enable the integration of actuating and sensing functions. As a proof of concept, the Janus film can serve as a self-supported device to simultaneously imitate the controllable contracting/expanding behaviors of the vocal sac of frog and monitor the real-time current change in this process, demonstrating significant potential in smart bionic applications.

KEYWORDS: hydrophilic/hydrophobic, bubble-like stretchable film, self-adhesive/self-adaptive, pneumatic, multifunctional electronics



the biomimetic behaviors through contraction, expansion, and more complicated motions.^{16,17} The soft muscle-like elastomers enable switchable actuating transformation from a two-dimensional (2D) planar surface to a three-dimensional (3D) expandable surface, demonstrating a wide range of interesting applications.^{16,18}

In nature, soft tissues can adapt themselves to dynamic environments in a real-time feedback and quick stimuli-

Soft materials, targeting smart and safe interactions with humans, are emerging as indispensable with the rapid development of artificial intelligence devices.^{1–6} Specifically, stretchable and flexible conductive elastomers have attracted tremendous consideration during the past few years owing to their significant and broad applications in stretchable/flexible electrodes,^{7–9} mechanical sensing,^{10,11} soft robots,^{12,13} etc. Typical examples of elastomers have served as not only ideal supporting targets but also active components to manipulate the conductive pathway embedded in the sensing devices.^{14,15} In addition, elastomers with ultrathin thickness could also be employed to function as pneumatic camouflaging skins or robotic actuators to imitate

Received: December 19, 2018

Accepted: April 10, 2019

Published: April 10, 2019

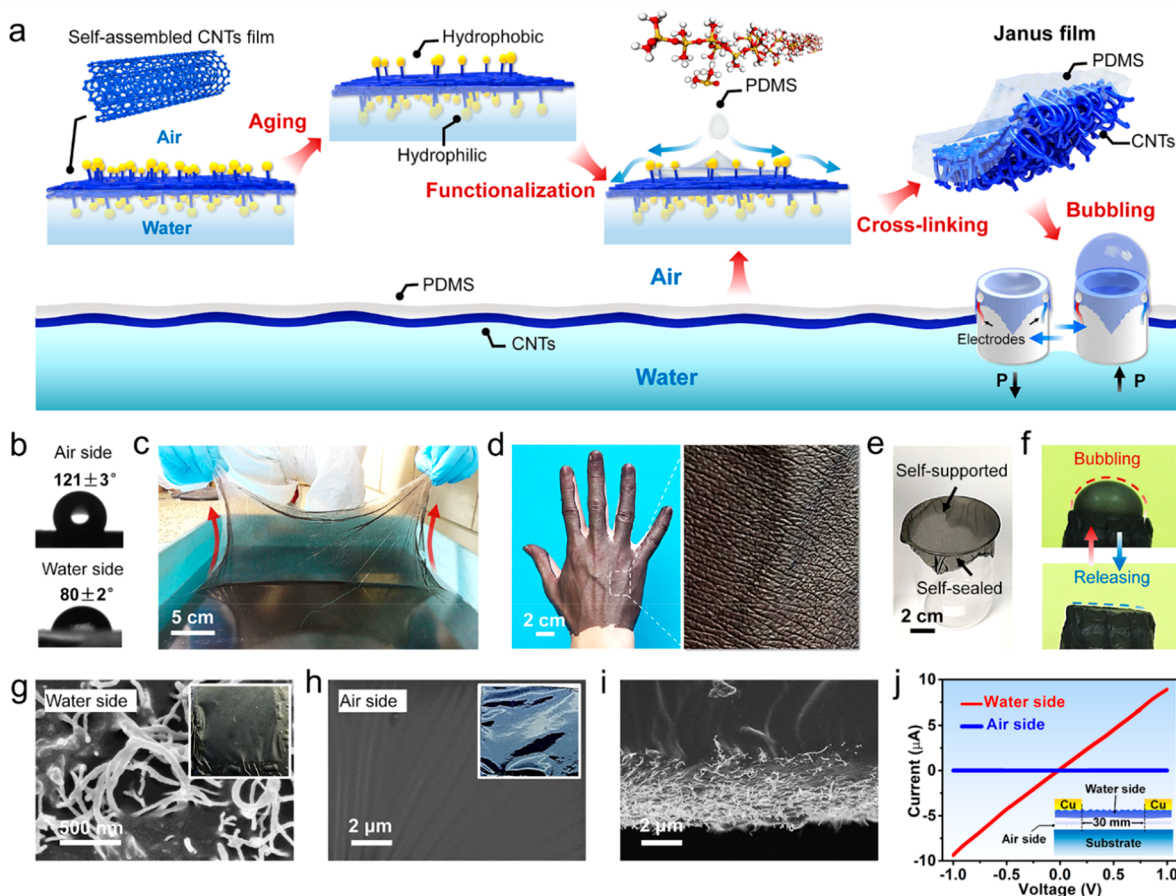


Figure 1. (a) Sketch of fabrication of bubble-like stretchable Janus ultrathin film at air/water interface through a hydrophilic/hydrophobic mediated asymmetric functionalization. (b) Water contact angle of air and water side of the self-assembled CNT film. (c) Photograph of large-area Janus hybrid film fabricated at air/water interface. (d) Film shows excellent self-adhesion and a high level of conformability on skin surface. (e) Self-supported film suspended on beakers. (f) Photos of the suspended Janus film could be blown into a bubble-like shape. SEM images of the as-prepared hybrid film surface of (g) water side layer with plenty of exposed CNT (rough surface) and (h) air side layer (smooth surface). (i) Amplified cross-sectional image of the self-supported CNT/PDMS film. (j) Current–voltage curves of the water and air side layers of the hybrid.

responsive way.¹⁷ In their system, the coordinated response of sensory perception and physical motions can effectively boost the adaptive process to a variable environment. Inspired by the living creatures, the alternative introduction of dielectric soft materials and conductive components into the design of actuating E-skins has played vital roles.¹⁹ More importantly, to accommodate complicated environments, mechanical compliance is deemed to be a prerequisite for actuating E-skins to realize multifunctional applications.^{20,21} Achieving stretchable E-skins with high conformability that can be actuated, however, is more challenging owing to the difficulty in the design and control of desirable 2D functional materials to match the aforementioned features.

At a molecular level surface, the aqueous (water-based) substrate is considered an ideal platform for self-assembly and interfacial physical/chemical reaction for functional 2D films under ambient conditions.^{20,22–28} Previously, Yu et al.²⁴ fabricated ultrathin free-standing hydrophilic/hydrophobic Janus films at the air/water interface *via* multilevel self-assembly. Qi et al.^{29,30} employed aqueous surface-mounted polystyrene microsphere films as templates for interfacial heterostructured metal film deposition. More recently, our group has developed a capillary force driving compression technique to self-assemble carbon nanotubes (CNTs) into a

closely packed conductive network at the air/water interface.^{31–33} Specifically, the assembled CNT films with hydrophilic groups can experience a subsequent aging process to achieve asymmetric wettability, demonstrating hydrophobic and hydrophilic properties at the air and water side, respectively.³⁴ The Janus properties of the CNT films can thus provide an active and robust platform for further asymmetric functionalization. Superior to the rigid substrate, the interfacial reaction behaviors based on the air/water interface could be easily manipulated, transferred, and scaled up.^{25,35–37}

Herein, we describe our recent advance to fabricate bubble-like stretchable Janus ultrathin films of asymmetric combination of CNT/PDMS with tunable microstructures and conductivity at the air/water interface. During this strategy, closely packed CNT film could be formed on the surface of water in large area through a Marangoni spread^{27,35–37} and capillary-force driving compression method.^{31,32} Significantly, the subsequent aging process can further induce the CNT film to realize hydrophobic and hydrophilic properties at the air and water side, respectively.³⁴ The asymmetric wettability thus can provide a functional platform for an *in situ* physical reaction. In our system, hydrophobic PDMS can unidirectionally functionalize the CNT layer at the air side, in which the

layer at the water side can be effectively protected to form a well-controlled Janus film. Significantly, the Janus hybrid film constructed at water surface endows it ultrathin, self-adhesive, self-adaptive, self-sealed, and even pneumatic properties. The combination of these excellent features can allow to realize unconventional and multifunctional applications, such as self-adhesive strain sensors/thermal management, noncontact sensing, and even bioinspired integration of pneumatic actuating/sensing.

RESULTS AND DISCUSSION

The ultrathin, conductive, and stretchable Janus hybrid film is fabricated by a typical CNT self-assembly at the air/water interface, hydrophilic/hydrophobic aging, and *in situ* interfacial asymmetric functionalization, which is schematically illustrated in Figure 1a. As previously reported by our group, the self-assembled CNT film with partially hydrophilic groups can further experience a subsequent aging process to achieve a steady state, resulting in hydrophobic and hydrophilic wettability at the air and water side, individually.³⁴ This asymmetric self-assembly system is considered to establish a significant foundation for subsequent *in situ* asymmetric modification. Note that the further development of an interfacial asymmetric functionalization strategy enables the controllable introduction of functional components into one side of the CNT film, resulting in desirable interfacial mechanical strength and multifunctional properties of the final Janus hybrid. On the basis of this robust method, a variety of units with functionality can be developed. In this work, as an active and functional platform, the CNT film with asymmetric wettability was further developed to construct Janus CNT/polymer-based films, which were expected to represent interesting microstructures and applications in smart soft materials. As a proof of concept, to further explore the potential applications in electronic skin and soft actuators, stretchable and flexible elastomers are introduced into the CNT films to realize a synergistic effect for multifunctional electronics. In our system, the resulting water contact angles of the air/water sides are $121 \pm 3^\circ$ and $80 \pm 2^\circ$, respectively (Figure 1b). Owing to the asymmetric wettability features of the CNT film, hydrophobic PDMS in hexane solution could be unidirectionally functionalized onto the air side layer of the CNT film, in which the other layer was effectively protected by the water. As a result, a CNT/PDMS-based Janus ultrathin film with asymmetric structure and conductivity can be readily achieved and be further cut, transferred, attached to various targets, and even employed as a free-standing one film realize integrated bubble-like actuation and simultaneous sensing behavior. As displayed in Figure S1, all of the targeted substrates are directly attached onto the air side of the achieved Janus film, resulting in the direct contact between the PDMS layer and substrate surface. The simple and robust *in situ* asymmetric decoration strategy allows us to fabricate a large-area film in the absence of complicated facilities under mild conditions (Figure S2), which could be readily lifted from the water surface without any breakage (Figure 1c). When attached onto the hand surface, the film represents excellent self-adhesive and self-adaptive properties (Figure 1d). The amplified image in Figure 1d clearly shows that the Janus hybrid film can follow smoothly along the epidermis and successfully duplicate the skin textures. More interestingly, the as-prepared film can also be transferred onto the brim of the beaker to support itself as a free-standing film, which can

adhere seamlessly to the beaker for a self-sealed system (Figure S3 and Figure 1e). Different from conventional conductive elastomer, the self-supported film in a sealed chamber could be pneumatically actuated into a well-controlled stretching state with apparent volume increase due to the ultrathin and stretchable properties. When the pressure in the chamber is released, the inflated film will recover to the initial state (Figure 1f). This specific feature allows us to explore and even realize some interesting applications, such as integrated pneumatic actuating/sensing devices. Attributed to the thicker thickness of the PDMS film formed at air/solid interface, it cannot readily adapt to the nonplanar targets. When the pure PDMS film fabricated by the conventional method was transferred onto the bottleneck, it did not spread seamlessly along the neck surface, resulting in an apparent void between the film and bottle surface, whereas the film fabricated at the air/water interface could adhere seamlessly onto the nonplanar surface (Figure S4a). Furthermore, the favorable features of the Janus ultrathin film can endure a relatively higher air pressure of ~ 1600 Pa than the conventional PDMS film with ~ 750 Pa. As shown in Figure S4b, our Janus film represented larger curvature of approaching ~ 0.8 cm⁻¹ than the conventional PDMS film with a curvature of about ~ 0.5 cm⁻¹. In addition, the resulted Janus film can experience higher air pressure with prominently macroscopic inflation. In addition, we also investigated the maximum self-sealing pressure of the film. In our experiments, a Janus film with a thickness of ~ 15 μ m was used to seal a three-necked flask and subsequently actuated by a series of air pressures. As a result, it can endure air pressure of up to ~ 2691 Pa in a desirable self-sealing condition (Figure S5). Note that the maximum endured pressure and curvature can be effectively adjusted by balancing the correlation between film thickness and adhesive force.

To further investigate the microarchitectures of the Janus film, SEM was performed to measure the morphology of both sides of the resulting film. As displayed in Figure 1g, the presence of the tubular structure of the water side with a rough surface ensures the conductive pathway of the film, which represents a distinct comparison with the smooth surface of the air side (Figure 1h). Moreover, Figure 1i and Figure S6 strongly evidence the asymmetric bilayer structure of the hybrid film. Significantly, the as-prepared film was endowed with asymmetrical electrical properties on the bottom and top layers, presenting maximum absolute current (copper tape electrodes with the width of 5 mm and interelectrode gap of 30 mm) of 9.3 μ A and 0.1 nA obtained at the bias of -1.0 and 1.0 V, respectively (Figure 1j). Furthermore, the mechanical strength of the PDMS with/without CNT modification was also investigated in Figure S7, in which the CNT film enhanced Janus film demonstrated distinctly enhanced failure strength and strain compared to that of the pure PDMS.

Interfacial self-assembly is considered as a preferable approach to construct modifiable and transferrable CNT film, which began with the homogeneous spreading of CNT/ethanol dispersion induced by Marangoni effect at air/water interface in high uniformity and efficiency. Superior to the conventional drop-coating method, a sprayer was adopted to homogeneously spread the CNT dispersion onto the water surface. The spray-coating method enabled the larger coverage area and higher efficiency than that of the drop-coating one. In addition, the sizes of the droplets can be prominently reduced from millimeters to micrometers, which can efficiently decrease the diffusion to the water phase. Due to the apparent difference

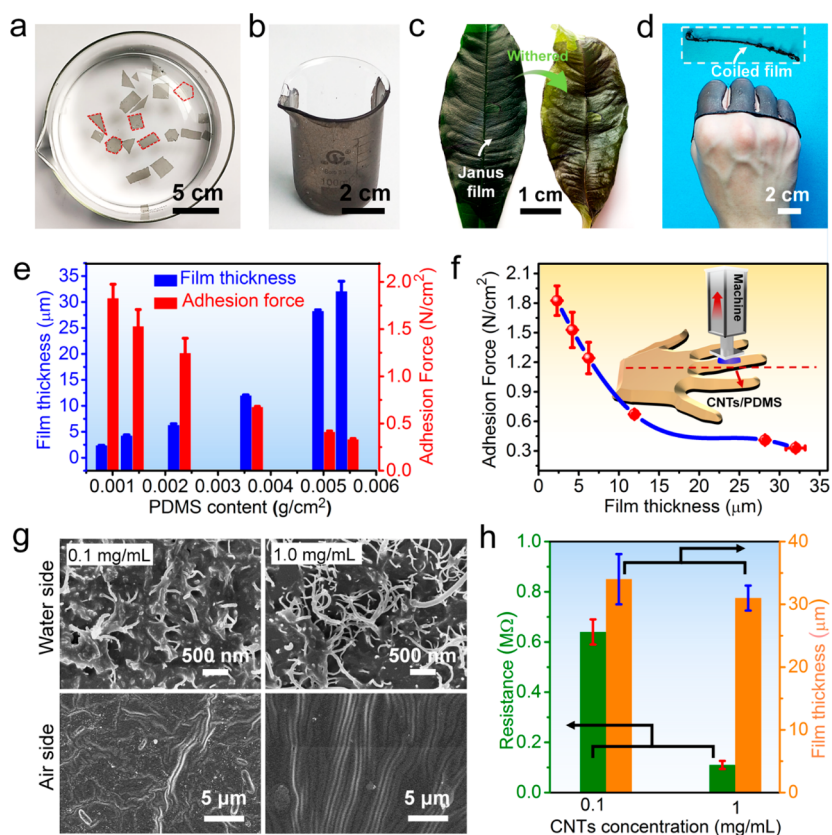


Figure 2. (a) Floating film can be readily tailored into diverse shapes. (b) Ultrathin and adhesive film can easily adhere onto the beaker surface. (c) Janus film can even be attached to a live leaf surface and maintain excellent adhesion after the leaf withers. (d) Film transferred onto hand surface can experience rigorous bending/releasing process and be easily peeled off without any residue after 2 h attachment (temp 23 °C, R.H. 78%). (e) Film thickness/adhesion force versus PDMS content column. (f) Adhesion force versus film thickness curve, demonstrating a negative correlation. (g) Resulting conductivity of the Janus film can be adjusted by changing the CNT concentration. (h) Resistance/film thickness versus CNT concentration column.

of surface tension between ethanol and water, the CNTs can be pushed outward rapidly from regions of lower surface tension to that of a higher one for homogeneous preassembled film.³⁶ It is noted that excess CNT dispersion can result in agglomeration phenomenon on the surface of preassembled CNT film, resulting in darker color than the other area of the film. Subsequently, a commercially available sponge with a pore size of about several tens of micrometers was employed to realize the final compression process. When the porous sponge was put on one side of the preassembled CNT film, a controlled compression of CNT film to a close-packed one could be readily realized, which was named as a capillary force driving compression method (Figure S8).³¹ The efficient and robust self-assembly process was characterized by SEM and AFM images, resulting in a closely packed tubular network (Figure S9). Additionally, Raman characterization was adopted to measure the carboxyl functionalized CNT films, demonstrating characteristic peaks of D, G, and 2D bands (Figure S10). Note that CNTs with hydrophilic groups are expected to be very important to achieve Janus CNT films with asymmetric wettability after subsequent aging process, which can act as a functional platform for further interface functionalization. It was observed that the freshly prepared CNT film had similar water contact angles, resulting in hydrophobic features on both sides of the film. To achieve an aging process, the as-prepared film at the air/water interface was placed in a sealed chamber with fixed humidity and temperature for an appropriate time

from 0 to 72 h. It is noted that the aging process allows the CNT film to have sufficient time to complete the secondary assembly. In this process, the Gibbs free energy was effectively decreased for a more stable state. As a result, more hydrophilic and hydrophobic groups of the film were exposed to the water and air phase, respectively. Significantly, the appropriate aging time under ambient conditions can ensure the formation of well-controlled wettability at air and water side of the CNT film. Owing to the incompatibility between the water and oil phase, when the hydrophobic PDMS/hexane mixture was spread onto the air side of CNT film, PDMS could not penetrate into the component parts of CNT film at the water side, allowing the formation of asymmetric hybrid film. The achieved Janus film at the air/water interface could be readily tailored into various shapes and attached onto arbitrary substrates, such as a glass beaker and even a live leaf (Figure 2a–c). Interestingly, the film is stable enough to spread along the refined textures of the fresh leaf and maintains a seamless attachment even after the leaf withers. Furthermore, Janus film transferred onto the hand surface can endure rigorous bending and releasing behaviors without any breakage. To preliminarily investigate film inflammation on human skin, the PDMS layer of a large Janus film was attached onto the back of the hand for the adhesion time ranging from 2 to 12 h at room temperature. Two important factors were considered in the tests, including any uncomfortable feelings of participants and painful inflammation on the skin. After a mechanical detachment of

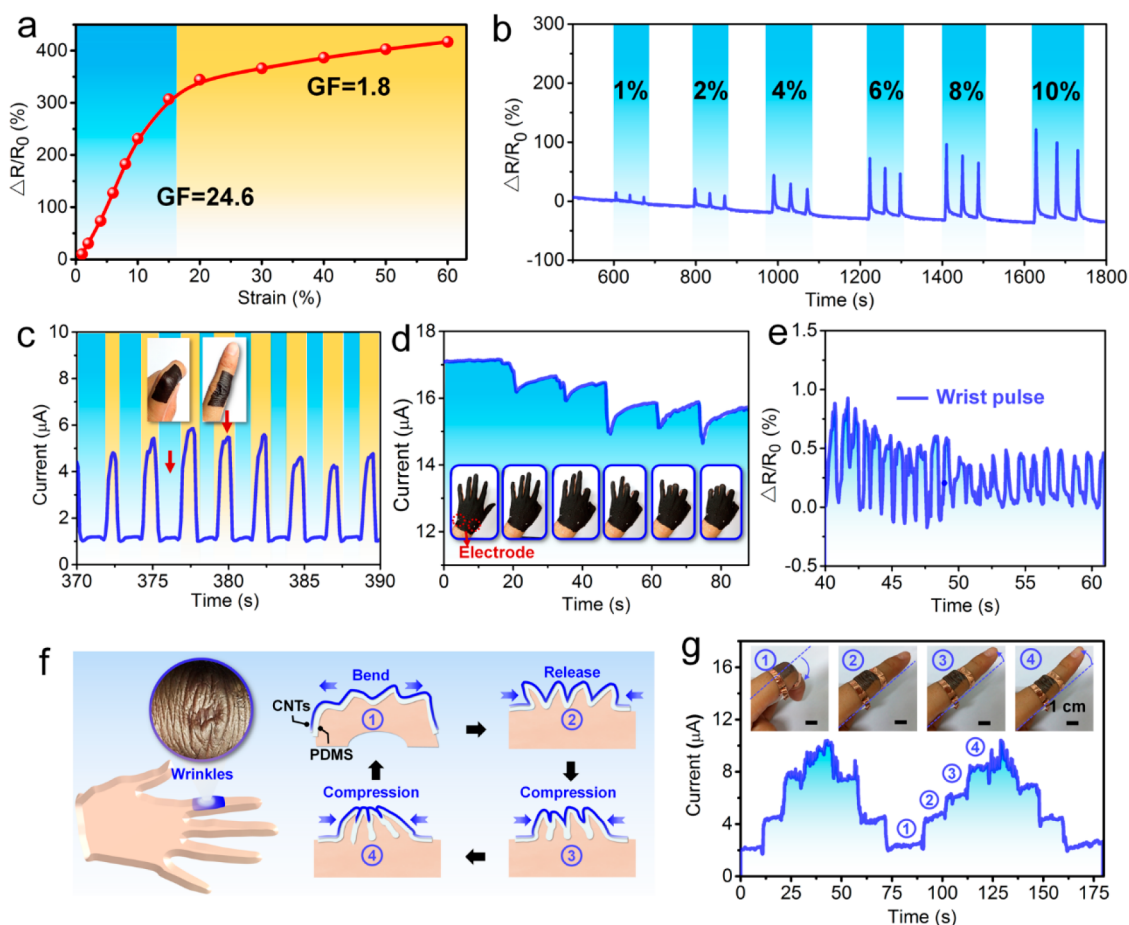


Figure 3. Epidermal strain sensor for human physiological behavior monitoring. (a) Resistance change *versus* applied strain. (b) Resistance change *versus* time under variable strain. (c) Real-time monitoring the bending and releasing behaviors of the finger. (d) Real-time detection of different finger motion behaviors. (e) Pulse signals detected by the self-adhesive epidermal electronics attached onto the wrist. (f) Schematic representation of the mechanism of epidermal electronics. (g) Electric signal of slight finger behavior. Inset: photos of finger-moving behavior.

the film from the skin surface no obvious negative effects, such as inflammation and discomfort, were observed on the skin (Figure 2d and Figure S11). Nevertheless, the current tests conducted are immature, and more refined factors are not considered. In future work, dermatitis evaluations achieved by the patch test criteria of the International Contact Dermatitis Research Group (ICDRG) and other relative tests will be conducted to explore the potential applications in epidermal electronics. Since there is a negative correlation between the flexibility and film thickness, thinner film can ensure more conformal contact and better adhesion to the topological skin. The thickness of the film can be efficiently adjusted by tuning the addition of the PDMS. As displayed in Figure 2e, when PDMS content increased, the film thickness and adhesion force demonstrate increasing (from 32 ± 2 to $2.3 \pm 0.1 \mu\text{m}$) and decreasing (from 1.8 ± 0.15 to $0.33 \pm 0.01 \text{ N/cm}^2$) tendency, individually.

The result shown in Figure 2f strongly evidence the inverse correlation between adhesion force and film thickness.³⁸ However, it is noted that films with a thickness of 2.3 and $4.7 \mu\text{m}$ representing a relative low strength cannot be entirely peeled off from the skin surface, resulting in a potential risk of inflammation (Figure S12). In order to maintain the high-adhesion and well-controlled delamination, film with thickness of about $12.5 \mu\text{m}$ is adopted in our system. In addition, the

conductivity of the Janus film could be alternatively tuned through adjusting the CNT concentration for CNT films with controllable thickness. As displayed in Figure S13 and Figure 2g, compared with the Janus film with low concentration of 0.1 mg/mL, more CNTs were exposed to the PDMS surface in the high concentration sample with 1 mg/mL. As a result, the acquired Janus film represented distinctly improved conductivity, which derived from the increased entanglement of the CNT network (Figure 2h).

As shown in Figure 3a, sensing performance of the as-prepared film was further explored, in which a monotonic curve with two distinct stages was clearly observed. When the sample was stretched to certain tensile strain (ϵ , $\epsilon = (l - l_0/l_0)$), the normalized relative resistance ($\Delta R/R_0$, $\Delta R/R_0 = R - R_0/R_0$) represented a gradual increase. The gauge factor (GF), which is defined as the relative ratio of ($\Delta R/R_0$) to ϵ , is estimated to be 24.6 ($\epsilon: \leq 15\%$) and 1.8 ($\epsilon: 15\text{--}60\%$), respectively. The real-time variation in the resistance of the film under repetitive stretching (from $\epsilon = 1, 2, 4, 6, 8$ to 10%) is displayed in Figure 3b, which indicates a good response to different tensile strain. Significantly, when the film was attached to the finger surface, the bending and releasing behaviors can be quantitatively monitored by the epidermal strain sensor (Figure 3c). Note that the epidermal device can even endure up to 1000 times bending and expanding cycles

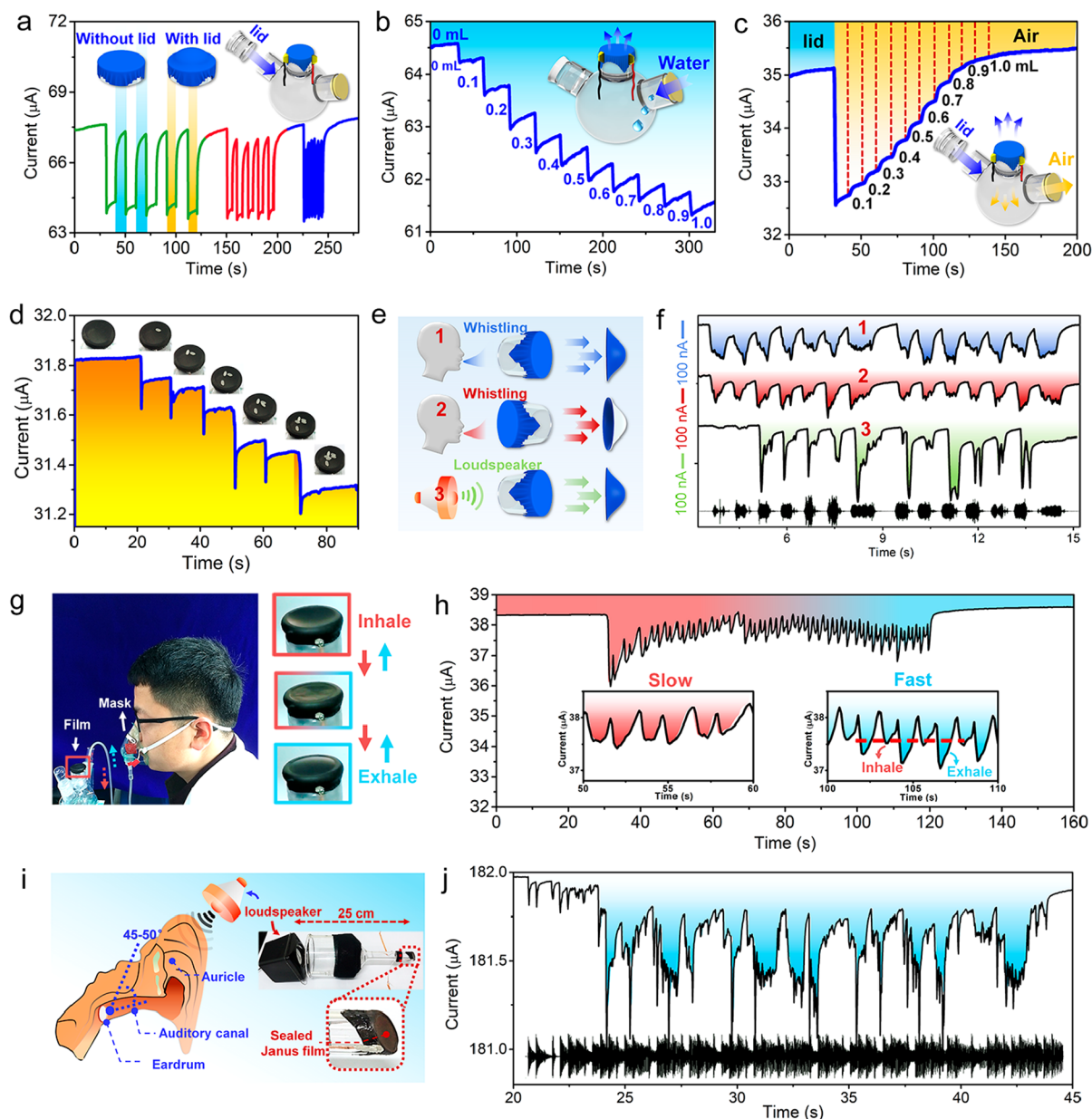


Figure 4. Self-supported Janus film of noncontact sensing performance. (a) Current *versus* time curve with/without lid covering on the flask. (b) Current change *versus* time with increasing the amount of water droplets. (c) Real-time detecting the covering the lid on the flask and then extracting the air inside the flask. (d) Self-supported sensor can be further adopted to detect the pressure change of the rice. (e) Sketch of whistling and loudspeaker induced air flow to drive the film vibration. (f) Current change *versus* time curves when the volunteer whistles from different direction and loudspeaker plays from one direction. (g) Photo of a homemade device with a self-supported film covering onto the flask, which can be employed to monitor human breath and schematic of the working mechanism of the device during the breathing process. (h) Real-time current change *versus* time when the volunteer breathes. (i) Schematic representation of the homemade acoustic detector to simulate the function of ear. (j) Real-time collected electrical waveform with the musical signal.

without any observed delamination and increase of resistance (Figure S14). As a proof of concept, a large-area film was transferred onto the entire hand, which could be used to realize a real-time monitoring of multiple finger motion behaviors. As shown in Figure 3d, the current signal demonstrates a gradual decrease with the successive bending of different fingers (from thumb, index, middle, ring, to little finger). Additionally, more subtle physiological signal could also be detected. Figure 3e shows the real-time arterial pulse waveform, in which distinguished peaks could be clearly observed. More importantly, due to the highly conformal attachment, even tiny finger motion can be precisely captured by this epidermal

system. Other than the downward bending of the finger with high strain (more than 30%), it is difficult to detect the tiny change of upward bending. Since the wrinkled skin can have a step-by-step contact in different stages of the upward bending, the real-time detection could be effectively achieved through the continuous contact of conductive components that self-adhered to the wrinkles of the skin (Figure 3f,g). Additionally, it is noted that the temperature can also have a significant effect on the conductivity of the Janus films, demonstrating a positive correlation with the current signals (Figure S15). However, there are considerable differences in the time scale between mechanical deformation and ambient temperature.

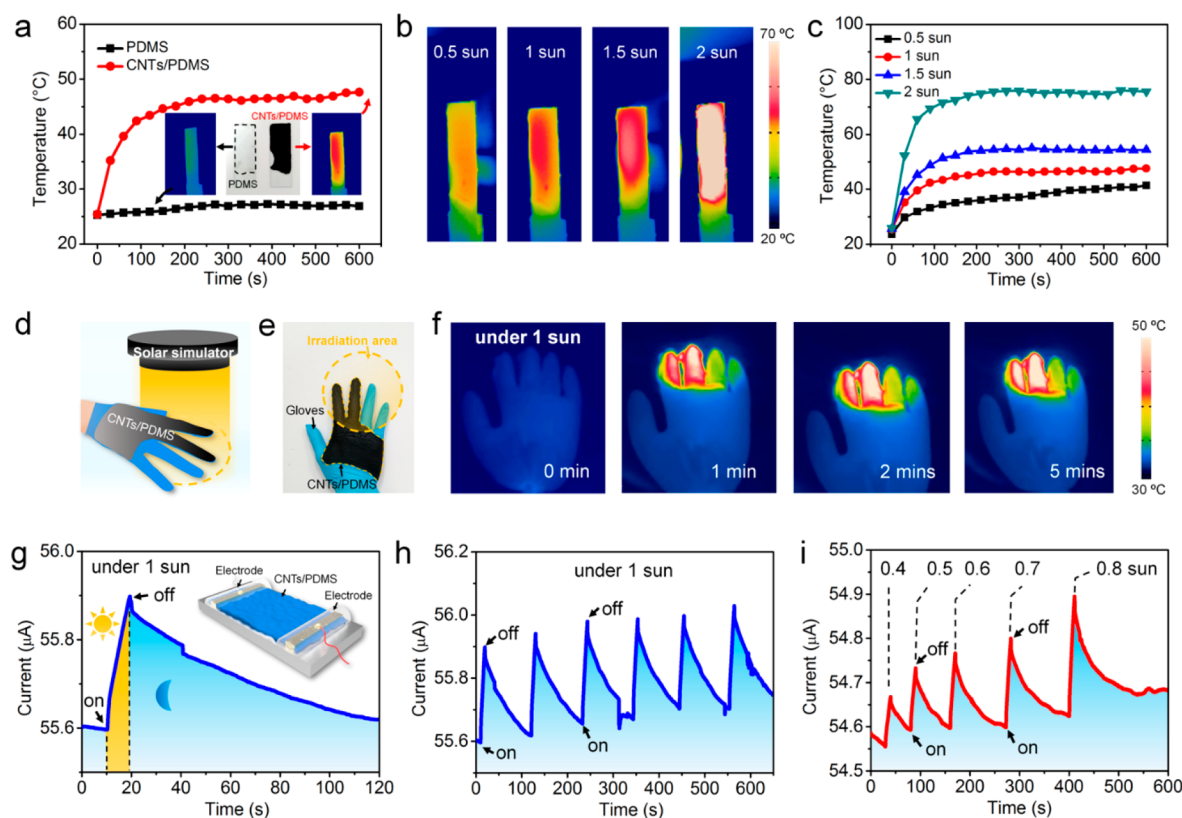


Figure 5. Self-adhesive thermal management and photoresponsive application. (a) Temperature *versus* time curves of PDMS and Janus CNT/PDMS films. (b) IR images of Janus film at varied solar intensity. (c) Temperature *versus* time curves of Janus films at different solar intensity. (d) Sketch of Janus film alternatively adhered onto the glove surface. (e) Optical image of Janus films on glove surface. (f) IR images of the Janus film under 1 sun. (g) Real-time current *versus* time curve with and without solar light. (h) Cycle experiment of the solar responsive behaviors. (i) Current *versus* time curve under different solar intensities.

Moreover, a control experiment was also conducted to investigate the temperature effect on the strain-sensing performance. As shown in Figure S16, two samples from the same Janus film were transferred onto the glass surface and bottleneck for a self-supported one, respectively, which were both placed in a room with certain temperature and humidity. It was observed that compared with the apparent current signal of the inflated film, no current change was detected in the control sample with no inflation. Generally, the change of ambient temperature is a relatively slow process; as a result, it will not distinctly affect the performance of the strain sensors.

Differing from conventional strain sensors, the noncontact strain behaviors can be successfully detected due to the self-adhesive and self-sealed features. For instance, the air pressure change inside a sealed system could be precisely detected. When the film was attached onto the edge of the flask to form a self-supported film (Figure S17), the behavior of covering the lid could induce an apparent bulge of the film, which can be precisely detected (Figure 4a and Figure S18). Owing to the high sensitivity of the film, even the injection of small amount of water droplets (0.1 mL) can be effectively monitored, presenting a stepped current decrease with a step-by-step water increase (Figure 4b). Moreover, when a lid was put on the flask, a gradual air extraction process inside the flask could be well-recorded, indicating potential applications in physical/chemical reaction monitoring inside a sealed system (Figure 4c). In addition, the noncontact sensors can also respond to the temperature changes due to temperature-induced air volume expansion mechanism. In our system, the film sealed

bottle was successively immersed into water bath at certain temperatures. As displayed in Figure S19, the film experienced a sunken process due to the air shrinkage below room temperature. With the increase of temperature, a bulge process happened to the film ranging from sunken, flat to bloated state, which could be reflected by a real-time current change. Due to the high-sensitivity of our ultrathin film, sunlight (Figure S20) and even body temperature can significantly drive the film to bulge with apparent signal output (Figure S21).

Furthermore, as a proof of concept, a homemade model is designed as a visual alarm to monitor the temperature change (Figure S22a). When the temperature is above 70 °C, the film will experience a large deformation, resulting in the conductive layer contacting with the electrodes to form a conductive circuit. Thus, the lighted LED can warn people of the high temperature for preventing potential accident (Figure S22b). Enlightened by this temperature-responsive air expansion, a light-driven actuator was developed to realize a well-controlled actuation behaviors (Figure S23). More importantly, the weight detection induced by film deformation was also realized. An example of detecting pressure change is presented in Figure 4d, where a stepped current change is observed with the gradual addition of rice. Note that the pressure induced by the weight of a grain of rice (about 20 mg) is only 0.53 Pa. Interestingly, an insect movement can also be detected by the pressure-induced current change in real time (Figure S24). Another potential application is showcased in Figures S25 and S26 and Figure 4e, in which a single word, sentence, and whistled tune can be precisely captured through the rhythmical

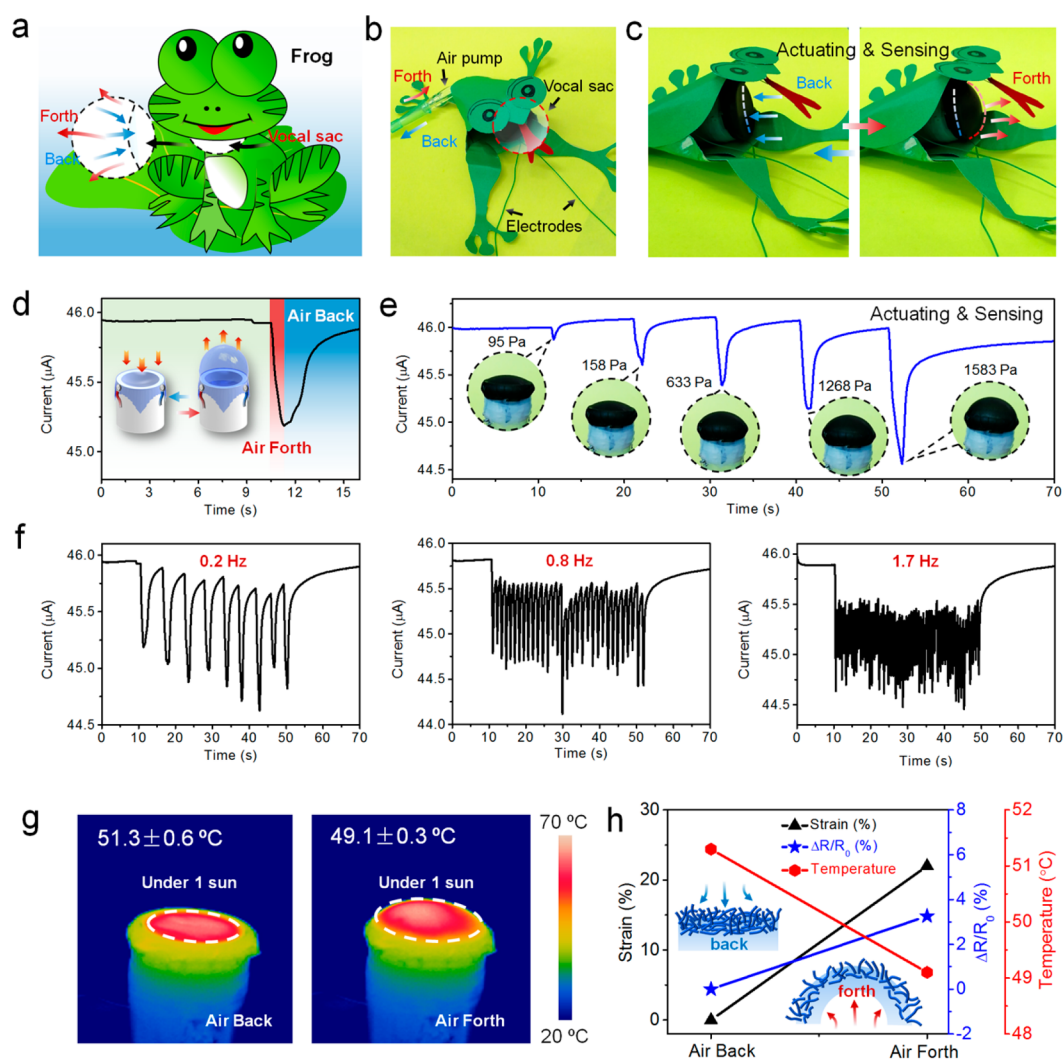


Figure 6. Bioinspired application to mimic the pneumatic actuating behavior of the vocal sac of a frog and simultaneous real-time monitoring. (a) Schematic of a male frog with its flexible vocal sac back and forth movement. (b) Artificial frog with Janus hybrid film as a flexible vocal sac. (c) Artificial vocal sac can be precisely controlled to conduct back/forth behavior by air pressure. (d) Real-time current signal monitoring of the back/forth process. (e) Dynamic behavior of the vocal sac actuated by a series of air pressures can be electrically recorded. (f) Flexible vocal sac can experience a series of slow and fast response/recovery cycles with different frequencies. (g) IR images of Janus film in air back and forth state under 1 sun, indicating a distinct temperature decrease after air forth. (h) Air back/forth cycle can apparently break the conductive CNT network, resulting in the decrease of conductivity and temperature.

vibration of the flexible film. Even whistling from the opposite direction could demonstrate the same characteristic patterns of the tune “Twinkle Twinkle Little Star”, indicating a good response to the air flow. When the whistled tune was recorded and played through the loudspeaker in a remote way, it also showed similar electrical signal changes (Figure 4f). The above result has encouraged us to further improve the signal detection system, indicating a significant potential in collecting acoustic vibrations.

The self-supported film also enables human health monitoring applications, such as real-time monitoring of respiratory rate. As shown in Figure 4g, the physiological breath signal can be indirectly monitored while breathing normally using the homemade detecting system. The concave and convex state of the film results from the inhaling and exhaling process, respectively, which can significantly drive the film stretching to certain strain for specific current change (Figure 4h). In particular, as breathing went on, the oxygen inside the bottle decreased gradually. Breathing may

experience a transition process ranging from a slow to fast state, which can be effectively recorded during the whole slow and fast breathing cycles. Inspired by the human ear, which is composed of an auricle, auditory canal, and eardrum, a homemade artificial ear is well-designed to imitate the functions of the ear illustrated as in Figure 4i. Even when the ultrathin film sensor was 25 cm away from the loudspeaker, a reliable current change could be accurately resolved, in which both the amplitude and frequency of acoustic vibrations were nearly consistent with the original signals (Figure 4j and Figure S27). The preliminary exploration in artificial ear will shed light on the applications of the eardrum-like ultrathin film.

As a renewable and sustainable resource, solar energy has aroused considerable interests in the field of energy storage, remote manipulation, and photothermal conversion. Among the family of wearable electronics, the flexible on-skin heating devices are promising and beneficial for thermal treatment. It is possible that solar light is regarded as an attractive trigger to realize *in situ* heating with power free. Since the as-prepared

Janus hybrid film with CNTs exposed to the air side can significantly absorb light to achieve a high-efficient solar-to-thermal conversion, it can be further employed as self-adhesive and flexible heating devices. As shown in Figure 5a, compared with the blank PDMS film on glass substrate with $\sim 27^\circ\text{C}$, the Janus one demonstrates higher temperature of $\sim 47^\circ\text{C}$ under 1 sun, which can be clearly observed in the corresponding IR images (Figure 5b). When the solar intensity is adjusted from 0.5 to 2 kW/m^2 , the balanced temperature can experience an apparent increase process ranging from ~ 40 to $\sim 74^\circ\text{C}$ (Figure 5c).

In our system, the CNT/PDMS film at the air/water interface was alternatively transferred onto the glove surface and irradiated under solar simulator (Figure 5d). The picture in Figure 5e clearly shows the obvious color contrast, resulting in differentiated solar absorption. With the increase of illumination time, two fingers with Janus film represent distinct temperature improvement of about $\sim 48^\circ\text{C}$ in the IR image in 5 min (Figure 5f). Note that to maintain a uniform surface the gloves were inflated with air. In addition, the illumination behavior can be effectively detected by the current change due to the potential photoelectric effect of the exposed CNTs. As displayed in Figure 5g, the conductivity of Janus film can experience a rapid increase process under 1 sun illumination and recover to the original state. This on/off illumination cycles could be readily achieved and effectively adjusted by changing the solar intensity (Figure 5h). As illustrated in Figure 5i, when increases the relative solar intensity, the photoresponsive current has a step by step increase process, demonstrating significant potentials to act as solar-energy charged thermal management devices.

Since the flexible and stretchable Janus ultrathin film enables the formation of self-supported and self-sealed system, it can be further adopted to realize the integration of actuating/sensing behaviors. In nature, some specific physiological structures of the animals have inspired us to develop bionic materials. For instance, the vocal sac of the male frog can experience an apparent bulge behavior, which derives from the air inside the lungs expelled into the vocal sac. The typical bulge of the flexible vocal sac can efficiently resonate with the sound to amplify the call (Figure 6a). As a proof of concept, a homemade artificial frog was equipped with a flexible Janus film, which functioned as a vocal sac combined with simultaneously actuating and sensitive sensing functions (Figure 6b). In this system, an air pump was employed to manipulate the Janus film to achieve an actuating behavior (back and forth state) (Figure 6c). In our system, a series of air pressures ranging from tens to thousands of Pa was employed to drive the film with a thickness of $\sim 15\ \mu\text{m}$ to have reversible inflation behaviors. As shown in Figure S28, the current signals could experience a controllable change under the applied pressure. Furthermore, there is a positively correlation between the actuating force and applied pressure. The actuating force of the pneumatic actuators can be effectively adjusted ranging from 0.05 to 0.55 N with favorable cycling performance. Note that the maximum value of the actuating force can be further elevated by alternatively balancing the film thickness and adhesion property. To maintain a stable self-sensing actuating behavior, the bandwidth can reach up to about 9 Hz at an actuated pressure of about 160 Pa (Figure S29). Specifically, with the increase of the applied pressure, the bandwidth of the actuators is expected to experience a decreased tendency due

to the increasing time required to accomplish one specific behavior.

To imitate the behavior of the vocal sac of the frog, air was pumped into the sealed chamber, and the Janus film experienced an obvious bulge process, resulting in quick response of the current signal (Figure 6d). It means that the actuating behavior of air back and forth can be successfully realized and real-time monitored. In addition, the stretchable film in different bulge level could also be detected, demonstrating potential applications in real-time monitoring the actuating behaviors (Figure 6e).

Furthermore, the Janus film represented excellent response performance in different frequencies ranging from 0.2 to 1.7 Hz (Figure 6f). Interestingly, attributed to the reduction of CNT entanglement and during the bulge process, the temperature of the film surface decreased from 51.3 to 49.1 $^\circ\text{C}$ under 1 sun, which was detected by IR images in Figure 6g. Note that when the artificial vocal sac experienced typical back and forth behavior, this process could be effectively and simultaneously detected by the current and temperature. Owing to the stretch-induced CNT disentanglement effects, the conductivity and temperature can have a decrease process, indicating significant potentials in real-time and multichannel feedback of the bionic behaviors (Figure 6h). Interestingly, owing to the favorable features of the stretchable Janus films, some biomimetic applications can be also realized. For example, the Janus film attached onto a specific chamber can function as a bionic swimming bladder of a fish to achieve a well-controlled movement behavior in water. When the Janus film attached chamber was immersed into the bulk water, the pressurized/unpressurized behaviors effectively drove the chamber to have a controllable movement. Note that the inflation behavior of the film can break the force balance on the chamber and the recovering process results in force rebalance of the chamber (Figure S30a). As displayed in Figure S30b, a homemade device with the Janus film packaged by PDMS was employed to manipulate the bionic swimming bladder to realize an up-and-down motion, demonstrating significant potentials in multifunctional actuators.

CONCLUSIONS

In conclusion, we presented a hydrophobic/hydrophilic mediated interfacial asymmetric functionalization approach for constructing Janus hybrid films of CNT/PDMS with ultrathin, stretchable, self-adhesive, and self-adaptive properties. The achieved Janus film could be further transferred onto arbitrary substrates with excellent self-adhesion, which can function as self-adhesive epidermal strain sensors and thermal management devices. Furthermore, the ultrathin and stretchable Janus film can be employed as a self-supported film to achieve unconventional noncontact sensing. Significantly, inspired by the vocal sac motion behavior of frog, it can further act as a pneumatic actuator with cycled bubbling behaviors, which can be simultaneously monitored by the deformation-induced signal change of current and temperature to achieve integrated multifunctional electronics.

EXPERIMENTAL METHODS

Materials. The raw carbon nanotubes (CNTs) (diameter, about 10–30 nm; length, about 10–30 μm ; $-\text{OH}$ %, about 2 wt %) with a purity of over 90% were acquired from Chengdu Organic Chemistry Co., Ltd., and were rinsed thoroughly with anhydrous ethanol and dried in a stream of nitrogen before use. PDMS films were fabricated

from Sylgard 184 (the ratio between component A and B was 1:10). Prior to film formation, the PDMS and corresponding cross-linker were diluted using hexane with a weight ratio of 4%. General chemicals in chemical reagent grade were used as received from Sinopharm Chemical Reagent. Ethanol and deionized water were used as rinsing solvents. Silicon wafers were cleaned in a mixture of $\text{H}_2\text{O}_2/\text{H}_2\text{SO}_4$ (1:3,v/v) at 80 °C (“piranha solution”) for 2 h and washed thoroughly with Milli-Q-grade water (Caution: Piranha solution reacts violently with organic matter!).

Preparation of CNT Film. First, the CNTs with $-\text{COOH}$ groups were dispersed with anhydrous ethanol, followed by ultrasonication for several hours. The ethanol-assisted carbon materials suspensions were spread onto the water surface by a spray-coating method for the appropriate volume, resulting in a uniform preassembled film formed at the air/water interface. To achieve a homogeneous one, the volume of CNT dispersion is very important. With the increase of CNT dispersion, the surface tension of the water surface can experience a gradual decrease process. When the irreversible agglomeration phenomenon was observed on the film surface, the spray-coating was stopped. It is noted that the location of the sprayer should be orderly changed for a homogeneous spreading during the spray-coating process. Prior to compression, a continuous water gap along the wall of the container was achieved by gently dropping the mixture of ethanol and water. Subsequently, a porous sponge was used to put on one side of the interface to quickly siphon water from the system, followed by a prominent decrease of the preassembled CNT film area. Notably, the homogeneous preassembled CNT film was closely packed toward the opposite direction of the siphone direction. When the move behavior of the film stopped and further siphone cannot drive the film, the resulting film is ultimately formed. According to previous work³⁴ in our group, further aging procedure is considered to play an important role in the formation of CNT film with asymmetric wettability at air/water interface. The self-assembled CNT film at air/water interface was further put in a sealed chamber with an average temperature of about 25 °C ranging from 0 to 72 h. Finally, the CNT film with aging time of 72 h was used to conduct the interfacial PDMS modification experiments.

Preparation of CNT/PDMS Ultrathin Film. A mixture of PDMS and hexane was sprayed onto the surface of the as-prepared CNT film to achieve a uniform layer, followed by a typical PDMS curing process (at 70 °C for 2h).

Characterization. Transmission electron microscopy (TEM) was recorded by a transmission electron microscope (JEM-2100F, accelerating voltage of 200 kV). TEM samples were prepared by dropping a diluted aqueous solution of CNT onto carbon-coated copper grids and dried in air. Atomic force microscopy (AFM) images were taken by a multimode AFM (Being Nano-Instruments, Ltd.) operating in the contact and/or tapping mode using silicon cantilevers (spring constant: 0.15 N m^{-1} , resonant frequency: 12 kHz for cantilever of contact mode, spring constant: 3–40 N m^{-1} , resonant frequency: 75–300 kHz for cantilever of tapping mode). Field emission scanning electron microscope images were obtained with an FE scanning electron microanalyzer (Hitachi-S4800, 4 kV). Optical transmittance of the films was probed using UV–vis–NIR spectra, which were obtained with a TU-1810 spectrophotometer from Beijing Purkinje General Instrument Co., Ltd. in transmission mode. Raman measurements were performed at room temperature on a Raman system (inVia-reflex, Renishaw). The solid-state diode laser (532 nm) was employed as an excitation source with a frequency range of 3200–1000 cm^{-1} . The current–voltage characteristics and current changes for the strain sensors were recorded by a semiconductor parameter analyzer (Keithley 4200) and the CHI660E electrochemical system. Static water contact angles were measured at room temperature using the sessile drop method and image analysis of the drop profile by using the instrument (OCA-20, Dataphysics) with a charge-coupled device camera and an image analysis processor. An IR camera (Optris PI 400) with a resolution of 382 × 288 pixels was employed to realize a real-time recording of the surface temperature and IR images. The data was analyzed by the PI connect software.

ASSOCIATED CONTENT

Supporting Information

The Supporting Information is available free of charge on the ACS Publications website at DOI: 10.1021/acs.nano.8b09600.

Schematic illustration of CNT film fabrication, transfer, and further asymmetric modification; Raman, AFM and SEM characterization of the CNT film fabrication; photos and SEM image of the Janus ultrathin films; mechanical strength of the pure PDMS and Janus films; response behaviors to a series of applied air pressure; skin attachment test; temperature-response behavior of the Janus film; Janus film actuated by temperature, sunlight, infrared light, *etc.*; current signal of the Janus film stimulated by applied air pressure, sound, air flow, insect; bionic actuators in water (PDF)

AUTHOR INFORMATION

Corresponding Authors

*E-mail: tao.chen@nimte.ac.cn.

*E-mail: zhanglei@nimte.ac.cn.

ORCID

Peng Xiao: 0000-0003-2231-9824

Jiawei Zhang: 0000-0002-3182-9239

Youju Huang: 0000-0001-5815-9784

Shiao-Wei Kuo: 0000-0002-4306-7171

Tao Chen: 0000-0001-9704-9545

Notes

The authors declare no competing financial interest.

ACKNOWLEDGMENTS

We thank the Natural Science Foundation of China (51803226, 51573203), Key Research Program of Frontier Sciences, Chinese Academy of Sciences (QYZDB-SSW-SLH036), and Bureau of International Cooperation of Chinese Academy of Sciences (174433KYSB20170061), Postdoctoral Innovation Talent Support Program (BX20180321), China Postdoctoral Science Foundation (2018M630695), and Ningbo Science and Technology Bureau (2018A610108).

REFERENCES

- (1) Sun, J.-Y.; Keplinger, C.; Whitesides, G. M.; Suo, Z. *Ionic Skin*. *Adv. Mater.* **2014**, *26*, 7608–7614.
- (2) Rus, D.; Tolley, M. T. Design, Fabrication and Control of Soft Robots. *Nature* **2015**, *521*, 467–475.
- (3) Gorissen, B.; Reynaerts, D.; Konishi, S.; Yoshida, K.; Kim, J. W.; De Volder, M. Elastic Inflatable Actuators for Soft Robotic Applications. *Adv. Mater.* **2017**, *29*, 1604977.
- (4) Polygerinos, P.; Correll, N.; Morin, S. A.; Mosadegh, B.; Onal, C. D.; Petersen, K.; Cianchetti, M.; Tolley, M. T.; Shepherd, R. F. Soft Robotics: Review of Fluid-Driven Intrinsically Soft Devices; Manufacturing, Sensing, Control, and Applications in Human-Robot Interaction. *Adv. Eng. Mater.* **2017**, *19*, 1700016.
- (5) Wirthl, D.; Pichler, R.; Drack, M.; Kettlguber, G.; Moser, R.; Gerstmayr, R.; Hartmann, F.; Bradt, E.; Kaltseis, R.; Siket, C. M.; Schausberger, S. E.; Hild, S.; Bauer, S.; Kaltenbrunner, M. Instant Tough Bonding of Hydrogels for Soft Machines and Electronics. *Sci. Adv.* **2017**, *3*, No. e1700053.
- (6) Sun, J.-Y.; Zhao, X.; Illeperuma, W. R. K.; Chaudhuri, O.; Oh, K. H.; Mooney, D. J.; Vlassak, J. J.; Suo, Z. Highly Stretchable and Tough Hydrogels. *Nature* **2012**, *489*, 133–136.
- (7) Sekitani, T.; Noguchi, Y.; Hata, K.; Fukushima, T.; Aida, T.; Someya, T. A Rubberlike Stretchable Active Matrix Using Elastic Conductors. *Science* **2008**, *321*, 1468–1472.

- (8) Shi, L.; Zhu, T.; Gao, G.; Zhang, X.; Wei, W.; Liu, W.; Ding, S. Highly Stretchable and Transparent Ionic Conducting Elastomers. *Nat. Commun.* **2018**, *9*, 2630.
- (9) Matsuhisa, N.; Inoue, D.; Zalar, P.; Jin, H.; Matsuba, Y.; Itoh, A.; Yokota, T.; Hashizume, D.; Someya, T. Printable Elastic Conductors by *In Situ* Formation of Silver Nanoparticles from Silver Flakes. *Nat. Mater.* **2017**, *16*, 834–840.
- (10) Jeong, S. H.; Zhang, S.; Hjort, K.; Hilborn, J.; Wu, Z. PDMS-Based Elastomer Tuned Soft, Stretchable, and Sticky for Epidermal Electronics. *Adv. Mater.* **2016**, *28*, 5830–5836.
- (11) Drotlef, D. M.; Amjadi, M.; Yunusa, M.; Sitti, M. Bioinspired Composite Microfibers for Skin Adhesion and Signal Amplification of Wearable Sensors. *Adv. Mater.* **2017**, *29*, 1701353.
- (12) Morin, S. A.; Shepherd, R. F.; Kwok, S. W.; Stokes, A. A.; Nemiroski, A.; Whitesides, G. M. Camouflage and Display for Soft Machines. *Science* **2012**, *337*, 828–832.
- (13) Mosadegh, B.; Polygerinos, P.; Keplinger, C.; Wennstedt, S.; Shepherd, R. F.; Gupta, U.; Shim, J.; Bertoldi, K.; Walsh, C. J.; Whitesides, G. M. Pneumatic Networks for Soft Robotics that Actuate Rapidly. *Adv. Funct. Mater.* **2014**, *24*, 2163–2170.
- (14) Lipomi, D. J.; Vosgueritchian, M.; Tee, B. C. K.; Hellstrom, S. L.; Lee, J. A.; Fox, C. H.; Bao, Z. N. Skin-like Pressure and Strain Sensors Based on Transparent Elastic Films of Carbon Nanotubes. *Nat. Nanotechnol.* **2011**, *6*, 788–792.
- (15) Roh, E.; Hwang, B.-U.; Kim, D.; Kim, B.-Y.; Lee, N.-E. Stretchable, Transparent, Ultrasensitive, and Patchable Strain Sensor for Human-Machine Interfaces Comprising a Nanohybrid of Carbon Nanotubes and Conductive Elastomers. *ACS Nano* **2015**, *9*, 6252–6261.
- (16) Hines, L.; Petersen, K.; Sitti, M. Inflated Soft Actuators with Reversible Stable Deformations. *Adv. Mater.* **2016**, *28*, 3690–3696.
- (17) Pikul, J. H.; Li, S.; Bai, H.; Hanlon, R. T.; Cohen, I.; Shepherd, R. F. Stretchable Surfaces with Programmable 3D Texture Morphing for Synthetic Camouflaging Skins. *Science* **2017**, *358*, 210–214.
- (18) Siefert, E.; Reysat, E.; Bico, J.; Roman, B. Bio-Inspired Pneumatic Shape-Morphing Elastomers. *Nat. Mater.* **2019**, *18*, 24–28.
- (19) Chen, L.; Weng, M.; Zhou, P.; Huang, F.; Liu, C.; Fan, S.; Zhang, W. Graphene-Based Actuator with Integrated-Sensing Function. *Adv. Funct. Mater.* **2019**, *29*, 1806057.
- (20) Park, Y.; Shim, J.; Jeong, S.; Yi, G.-R.; Chae, H.; Bae, J. W.; Kim, S. O.; Pang, C. Microtopography-Guided Conductive Patterns of Liquid-Driven Graphene Nanoplatelet Networks for Stretchable and Skin-Conformal Sensor Array. *Adv. Mater.* **2017**, *29*, 1606453.
- (21) Kim, D.-H.; Lu, N.; Ma, R.; Kim, Y.-S.; Kim, R.-H.; Wang, S.; Wu, J.; Won, S. M.; Tao, H.; Islam, A.; Yu, K. J.; Kim, T.-i.; Chowdhury, R.; Ying, M.; Xu, L.; Li, M.; Chung, H.-J.; Keum, H.; McCormick, M.; Liu, P.; Zhang, Y.-W.; Omenetto, F. G.; Huang, Y.; Coleman, T.; Rogers, J. A. Epidermal Electronics. *Science* **2011**, *333*, 838–843.
- (22) Qin, B.; Zhang, S.; Song, Q.; Huang, Z.; Xu, J.-F.; Zhang, X. Supramolecular Interfacial Polymerization: A Controllable Method of Fabricating Supramolecular Polymeric Materials. *Angew. Chem., Int. Ed.* **2017**, *56*, 7639–7643.
- (23) Zhang, F.; Fan, J.; Zhang, P.; Liu, M.; Meng, J.; Jiang, L.; Wang, S. A Monolithic Hydro/Organo Macro Copolymer Actuator Synthesized *via* Interfacial Copolymerization. *NPG Asia Mater.* **2017**, *9*, No. e380.
- (24) Zhang, H. B.; Hao, R.; Jackson, J. K.; Chiao, M.; Yu, H. F. Janus Ultrathin Film from Multi-Level Self-Assembly at Air-Water Interfaces. *Chem. Commun.* **2014**, *50*, 14843–14846.
- (25) Wang, X.; Xiong, Z.; Liu, Z.; Zhang, T. Exfoliation at the Liquid/Air Interface to Assemble Reduced Graphene Oxide Ultrathin Films for a Flexible Noncontact Sensing Device. *Adv. Mater.* **2015**, *27*, 1370–1375.
- (26) Zhang, L.; Xiao, P.; Lu, W.; Zhang, J.; Gu, J.; Huang, Y.; Chen, T. Macroscopic Ultrathin Film as Bio-Inspired Interfacial Reactor for Fabricating 2D Freestanding Janus CNTs/AuNPs Hybrid Nanosheets with Enhanced Electrical Performance. *Adv. Mater. Interfaces* **2016**, *3*, 1600170.
- (27) Yun, T.; Kim, J.-S.; Shim, J.; Choi, D. S.; Lee, K. E.; Koo, S. H.; Kim, I.; Jung, H. J.; Yoo, H.-W.; Jung, H.-T.; Kim, S. O. Ultrafast Interfacial Self-Assembly of 2D Transition Metal Dichalcogenides Monolayer Films and Their Vertical and In-Plane Heterostructures. *ACS Appl. Mater. Interfaces* **2017**, *9*, 1021–1028.
- (28) Yu, M.; Zhang, Y.; Zeng, Y.; Balogun, M.-S.; Mai, K.; Zhang, Z.; Lu, X.; Tong, Y. Water Surface Assisted Synthesis of Large-Scale Carbon Nanotube Film for High-Performance and Stretchable Supercapacitors. *Adv. Mater.* **2014**, *26*, 4724–4729.
- (29) Wang, W.; Dong, J.; Ye, X.; Li, Y.; Ma, Y.; Qi, L. Heterostructured TiO₂ Nanorod@Nanobowl Arrays for Efficient Photoelectrochemical Water Splitting. *Small* **2016**, *12*, 1469–1478.
- (30) Li, Y.; Ye, X.; Ma, Y.; Qi, L. Interfacial Nanosphere Lithography toward Ag₂S-Ag Heterostructured Nanobowl Arrays with Effective Resistance Switching and Enhanced Photoresponses. *Small* **2015**, *11*, 1183–1188.
- (31) Xiao, P.; Gu, J.; Wan, C.; Wang, S.; He, J.; Zhang, J.; Huang, Y.; Kuo, S.-W.; Chen, T. Ultrafast Formation of Free-Standing 2D Carbon Nanotube Thin Films through Capillary Force Driving Compression on an Air/Water Interface. *Chem. Mater.* **2016**, *28*, 7125–7133.
- (32) Wang, S.; Xiao, P.; Liang, Y.; Zhang, J.; Huang, Y.; Wu, S.; Kuo, S.-W.; Chen, T. Network Cracks-Based Wearable Strain Sensors for Subtle and Large Strain Detection of Human Motions. *J. Mater. Chem. C* **2018**, *6*, 5140–5147.
- (33) Zhang, L.; Xiao, P.; Lu, W.; Zhang, J.; Gu, J.; Huang, Y.; Chen, T. Macroscopic Ultrathin Film as Bio-Inspired Interfacial Reactor for Fabricating 2D Freestanding Janus CNTs/AuNPs Hybrid Nanosheets with Enhanced Electrical Performance. *Adv. Mater. Interfaces* **2016**, *3*, 1600170.
- (34) Liang, Y.; Shi, J.; Xiao, P.; He, J.; Ni, F.; Zhang, J.; Huang, Y.; Huang, C.-F.; Chen, T. A Lotus-Inspired Janus Hybrid Film Enabled by Interfacial Self-Assembly and *In Situ* Asymmetric Modification. *Chem. Commun.* **2018**, *54*, 12804–12807.
- (35) Noh, J.; Jeong, S.; Lee, J.-Y. Ultrafast Formation of Air-Processable and High-Quality Polymer Films on An Aqueous Substrate. *Nat. Commun.* **2016**, *7*, 12374.
- (36) Gao, P.; He, J.; Zhou, S.; Yang, X.; Li, S.; Sheng, J.; Wang, D.; Yu, T.; Ye, J.; Cui, Y. Large-Area Nanosphere Self-Assembly by a Micro-Propulsive Injection Method for High Throughput Periodic Surface Nanotexturing. *Nano Lett.* **2015**, *15*, 4591–4598.
- (37) Li, X.; Yang, T.; Yang, Y.; Zhu, J.; Li, L.; Alam, F. E.; Li, X.; Wang, K.; Cheng, H.; Lin, C.-T.; Fang, Y.; Zhu, H. Large-Area Ultrathin Graphene Films by Single-Step Marangoni Self-Assembly for Highly Sensitive Strain Sensing Application. *Adv. Funct. Mater.* **2016**, *26*, 1322–1329.
- (38) Park, D. Y.; Joe, D. J.; Kim, D. H.; Park, H.; Han, J. H.; Jeong, C. K.; Park, H.; Park, J. G.; Joung, B.; Lee, K. J. Self-Powered Real-Time Arterial Pulse Monitoring Using Ultrathin Epidermal Piezoelectric Sensors. *Adv. Mater.* **2017**, *29*, 1702308.